Immune microenvironment and treatment response of dMMR gastric cancer: Heterogeneity and implications for immunotherapy

LIPING WANG[1*], XINLIANG ZHONG[1*], MENGXING DIAO[1*] and WEI DENG[2]

[1]Department of Medical Oncology, Southern University of Science and Technology Hospital, Shenzhen, Guangdong 518055, P.R. China; [2]Department of Pathology, Southern University of Science and Technology Hospital, Shenzhen, Guangdong 518055, P.R. China

Received June 10, 2025; Accepted November 13, 2025

DOI: 10.3892/ol.2026.15472

Abstract. Deficient mismatch repair (dMMR) in gastric cancer is associated with a high tumor mutation burden (TMB) and increased neoantigen load, which may enhance sensitivity to immunotherapy. Nevertheless, heterogeneous responses among patients with dMMR suggest complex tumor immune microenvironment (TIME) regulation. The present study aimed to integrate a case of dMMR gastric cancer with multi-cohort bioinformatic analyses to assess TIME determinants of immunotherapy outcomes, focusing on hematological immune cell subsets. Pre- and post-immunotherapy TIME changes were evaluated in a patient with dMMR gastric cancer using immunohistochemistry analysis [$CD8^+$, $CD4^+$, forkhead box P3 $(FoxP3)^+$ regulatory T cells (Tregs), M1/M2 macrophages and programmed death-ligand 1 (PD-L1)]. Moreover, bioinformatics analyses assessed microsatellite instability (MSI) status, immune checkpoints [cytotoxic T-lymphocyte-associated protein 4 (CTLA4), CD274 and programmed cell death protein 1 (PDCD1)], TMB and TIME cell infiltration across The Cancer Genome Atlas (TCGA)-stomach adenocarcinoma (STAD; n=383), Kim (n=45), Peking University Cancer Hospital (n=31) and Esophagogastric Cancer-Memorial Sloan Kettering-2017 (EGC-MSK-2017; n=28) cohorts using CIBERSORT (LM22) and R-based statistical approaches. The case report demonstrated that, prior to treatment, the tumor was deemed 'immune cold', characterized by low levels of $CD8^+$ T cells, M1 macrophages and Tregs. Post-treatment, total T cell infiltration increased, driven primarily by $CD4^+$ T cells, while $CD8^+$ T cell levels remained low. $FoxP3^+$ T cell density (0.18 cells/mm^2) indicated potential immune suppression; B cell infiltration ($CD20^+$, 17.07 cells/mm^2) did not markedly increase, with no tertiary lymphoid structures (TLS) detected. Moreover, bioinformatics cross-cohort analyses revealed favorable immunological features in microsatellite instability (MSI)-high (MSI-H) gastric cancer compared with in MSI-low (MSI-L)/microsatellite stability (MSS) gastric cancer. In TCGA-STAD dataset, MSI-H tumors had significantly higher TMB, neoantigen load, infiltration of memory-activated $CD4^+$ T cells, activated natural killer (NK) cells, mast cells, M1 macrophages and immune checkpoint markers (CTLA4, CD274 and PDCD1; all $P<0.05$); $CD8^+$ T cells differed significantly between MSI-H and MSI-L ($P<0.05$), but not between MSI-H and MSS cancer. MSI-H was associated with a higher TMB in the Kim and EGC-MSK-2017 cohorts, a higher immunotherapy response rate in the Kim cohort ($P<0.05$) and trends toward improved OS in TCGA-STAD [hazard ratio (HR), 0.68] and EGC-MSK-2017 (HR, 0.42) cohorts. All survival differences were non-significant ($P>0.05$). In conclusion, the results demonstrated that in dMMR/MSI-H tumors (which typically exhibit high TMB and neoantigen load), a TIME characterized by low $CD8^+$ T cells, high Tregs, absent TLS and low PD-L1, could be indicative of immunotherapy resistance. Cross-cohort analysis further revealed that despite favorable immunological features (higher TMB, neoantigen load, memory-activated $CD4^+$ T cells, activated NK cells, mast cells, M1 macrophages and immune checkpoint expression), MSI-H gastric cancers have heterogeneous immunotherapy outcomes. Collectively, dMMR/MSI-H status alone is insufficient for outcome prediction, highlighting the need for individualized TIME evaluation in patients with gastric cancer receiving immunotherapy.

Correspondence to: Dr Liping Wang, Department of Medical Oncology, Southern University of Science and Technology Hospital, 6019 Liuxian Avenue, Nanshan, Shenzhen, Guangdong 518055, P.R. China
E-mail: wlpwlp2005@126.com

*Contributed equally

Abbreviations: MMR, mismatch repair; dMMR, deficient MMR; pMMR, proficient MMR; TMB, tumor mutational burden; ORR, objective response rate; PFS, progression-free survival; TILs, tumor-infiltrating lymphocytes; PD-L1, programmed death-ligand 1; Treg, regulatory T cells; MDSC, myeloid-derived suppressor cells; TCGA, The Cancer Genome Atlas; MSI-H, MSI-high; MSS, microsatellite stability; NK, natural killer; VEGF, vascular endothelial growth factor; CPS, combined positive score

Key words: dMMR, gastric cancer, immune microenvironment, immunotherapy, immune escape, bioinformatics analysis

Introduction

Gastric cancer is a leading cause of cancer-related death, ranking fifth in incidence and third in mortality worldwide. In 2020, there were ~1.1 million new cases and ~769,000 deaths globally, with the highest rates observed in East Asia, Eastern Europe and

South America (1). China accounts for nearly half of the global burden, with particularly high incidence in rural provinces such as Gansu and Henan. Despite a decline in the age-standardized incidence rate (annual change of -0.41%), the absolute number of new cases has risen due to population aging and growth (2). Together, these trends reflect the need for improved prevention and treatment, especially in high-burden regions.

Deficient mismatch repair (dMMR) is a key molecular feature of gastric cancer, often associated with microsatellite instability (MSI)-high (MSI-H) status, resulting in genomic instability and a high tumor mutation burden (TMB) (3). This, in turn, increases tumor immunogenicity and enhances the likelihood of immune checkpoint inhibitors (ICIs) treatment response (4). In advanced gastric cancer, dMMR accounts for 7-10% of cases, most frequently in gastric body adenocarcinoma or elderly patients (5). Compared with proficient mismatch repair (pMMR), dMMR is generally linked with a better prognosis but reduced sensitivity to standard chemotherapy (5).

Clinical studies have confirmed that patients with dMMR gastric cancer respond better to ICIs compared with traditional treatments. Indeed, programmed death-1 (PD-1)/programmed death-ligand 1 (PD-L1) inhibitors have been reported to markedly improve objective response rates (ORR) and pathological complete response (pCR) rates (6). In one trial, the pCR rate was 57.9% in patients receiving neoadjuvant immunotherapy, compared with 0.0% in the chemotherapy group (7). In addition, combining immunotherapy with chemotherapy has been reported to prolong progression-free survival (PFS) (8). Consequently, dMMR and MSI-H have been established as key predictive biomarkers for immunotherapy and have received U.S. Food and Drug Administration approval for guiding treatment decisions (9).

Nevertheless, a subset of patients with dMMR gastric cancer still fail to benefit from immunotherapy. Factors such as the tumor microenvironment, genetic mutations, loss of neoantigens and acquired resistance may contribute to treatment failure. Notably, the tumor immune microenvironment (TIME) has emerged as a critical determinant of immunotherapy success. Research suggests that tertiary lymphoid structures (TLS) within the tumor can enhance response to ICIs by improving antigen presentation and activating T and B cells (10,11). Therefore, deciphering the immune microenvironment may help explain variability in patient responses and guide more effective treatment strategies.

The present study describes the clinical case of a patient with dMMR gastric cancer who, despite receiving a combination of immunotherapy and chemotherapy, had suboptimal treatment outcomes. Through analysis of the TIME before and after treatment, coupled with bioinformatics analysis of patients with dMMR gastric cancer, the present study aimed to identify factors influencing immunotherapy efficacy and explore how these insights can optimize future treatment strategies for patients with dMMR gastric cancer.

Materials and methods

Case source. The present case was sourced from the Department of Oncology at Southern University of Science and Technology Hospital (Shenzhen, China). The initial consultation date of the patient was in April 2022. The present study was approved by the Ethics Committee of Southern University of Science and Technology Hospital [approval no. 2023(12)], and the patient signed an informed consent form, agreeing that case information and test results from pre- and post-treatment specimens may be used for academic reporting. The standard treatment protocol strictly adhered to the 2021 Chinese Clinical Oncology Society Guidelines for the Diagnosis and Treatment of Gastric Cancer (12).

EBER in situ hybridization. EBER *in situ* hybridization was performed using the EBER Probe kit (Roche Diagnostics, cat. no. 05997704001) according to the manufacturer's instructions. Formalin-fixed paraffin-embedded sections (4 μm, fixed in 10% neutral buffered formalin at room temperature for 24 h) were first subjected to permeabilization with kit-supplied protease K (20 μg/ml in 1xPBS, room temperature, 5 min), followed by post-fixation with 1xPBS (room temperature, 1 min, 2 washes). Pre-hybridization was conducted with kit-provided buffer (without probe) at 37˚C for 30 min; then, hybridization was performed using the kit probe (diluted 1:50 in hybridization buffer, final concentration 2 ng/μl, 20 μl per section) in a humidified chamber at 37˚C for 16 h. Excess probe was removed via sequential washes with 2xSSC, 0.5xSSC, and 0.2xSSC (all at 48˚C, 5 min per wash). Post-hybridization steps included blocking with 5% BSA (cat. no. A7906; Sigma-Aldrich; Merck KGaA; room temperature, 10 min), incubation with anti-digoxigenin primary antibody (Roche Diagnostics, cat. no. 11093274910, 1:100 dilution, 37˚C, 30 min) and biotinylated goat anti-mouse IgG secondary antibody (Roche Diagnostics, cat. no. 11093074910, 1:200 dilution, room temperature, 20 min). Detection was carried out with DAB chromogenic substrate (Roche Diagnostics, cat. no. 11718096001, room temperature, 10 min), and images were captured using an Olympus BX53 light microscope (x200 magnification).

Immune microenvironment detection methods pre- and post-treatment. Multiplex immunofluorescence staining was performed by D Medicines (Shanghai) Co., Ltd. The primary antibodies included CD8, CD4, FoxP3, M1/M2 macrophage markers, and PD-L1; imaging was conducted with a Leica DM6 B microscope at x200 magnification. Scanned images of each slide were subsequently overlaid to generate a single composite image. The fluorescence images were then imported into the AP-TIME software (0.3.6; 3D Biotech Ltd.) for analysis. Pan-CK staining was used to distinguish between tumor parenchyma and stroma. The number of different cell populations was quantified by the number of stained cells/mm^2 and the percentage of positively stained cells among all nucleated cells. In the TIME Profiling (TIME-PRO) test, 'marge1' and 'marge2' refer to two different panoramic views or heat maps, illustrating the distribution and state of immune cells within the tumor microenvironment, and providing rich information concerning the immune landscape of the tumor.

Data sources and analysis methods

Non-immune treatment cohort. The gastric adenocarcinoma dataset was downloaded from The Cancer Genome Atlas (TCGA) database [TCGA-stomach adenocarcinoma (STAD)] (13), comprising 440 patients (portal.gdc.cancer.gov/). After filtering for cases with available MSI status, 383

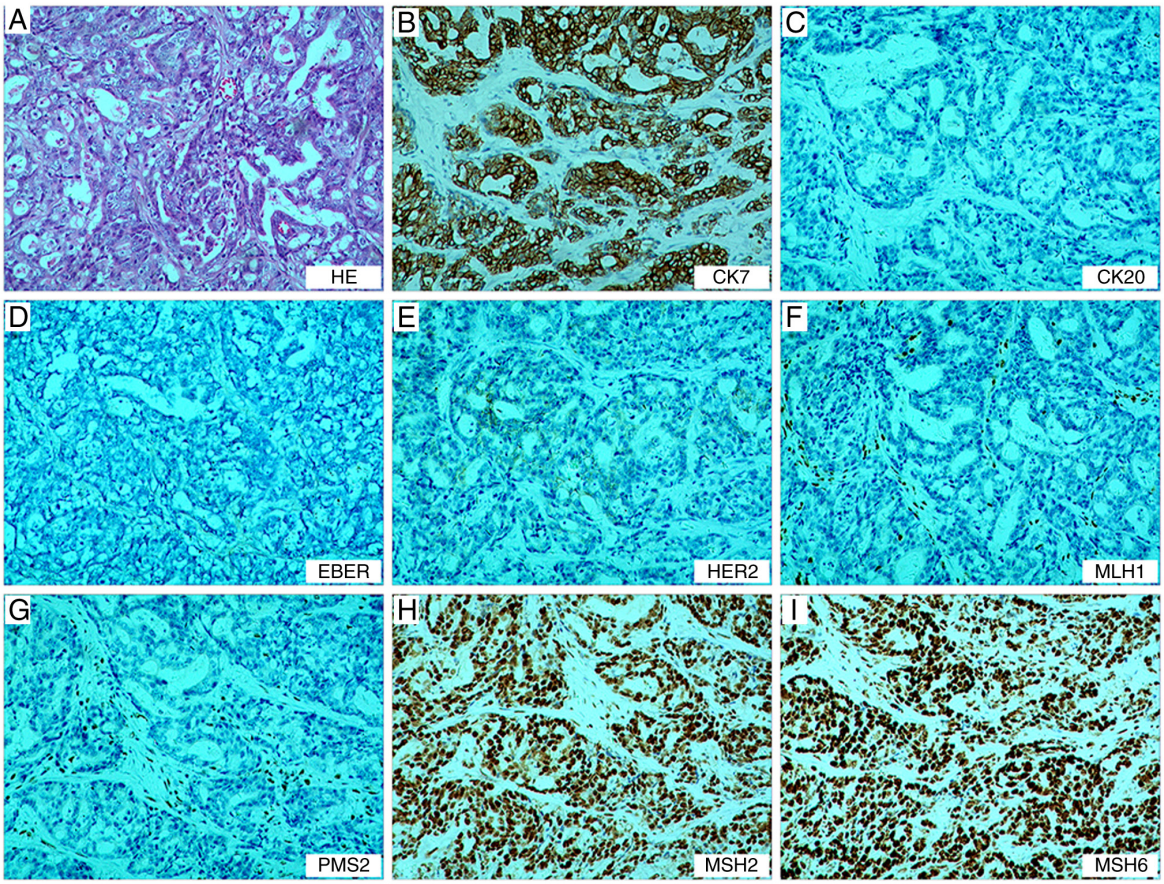

Figure 1. Postoperative pathological findings of the gastric tumor. (A) Tumor cells show diffuse/sheet-like growth with focal glandular differentiation, increased nuclear-to-cytoplasmic ratio and hyperchromatic nuclei. Immunohistochemistry demonstrates (B) CK7 (+), (C) CK20 (-), (D) EBER (-), (E) C-erbB-2 (0), (F) MLH1 (-), (G) PMS2 (-), (H) MSH2 (+) and (I) MSH6 (+), confirming deficient mismatch repair status. Magnification, x100. MLH1, MutL homolog; PMS2, postmeiotic segregation increased (*S. Cerevisiae*) 2; MSH, MutS homolog.

Table I. Immune microenvironment assessment results summary: Immune checkpoint expression levels.

A, Pre-treatment

	Count/mm^2, %			
Test index	Tumor parenchyma	Stroma	TPS, %	CPS
PD-1	0.00 (0.00)	0.00 (0.00)	-	-
PD-L1	-	-	<1	<1

B, Post-treatment

	Count/mm^2, %			
Test index	Tumor parenchyma	Stroma	TPS, %	CPS
PD-1	0.53 (0.01)	1.53 (0.02)	-	-
PD-L1	-	-	<1	<1

TPS, tumor proportion score; CPS, combined positive score; PD-1, programmed death-1; PD-L1, programmed death-ligand 1.

cases were retained. RNA sequencing data in transcripts per million format was extracted. Among these cases, 75 were classified as MSI-H, 52 as MSI-low (MSI-L) and 256 as microsatellite stability (MSS).

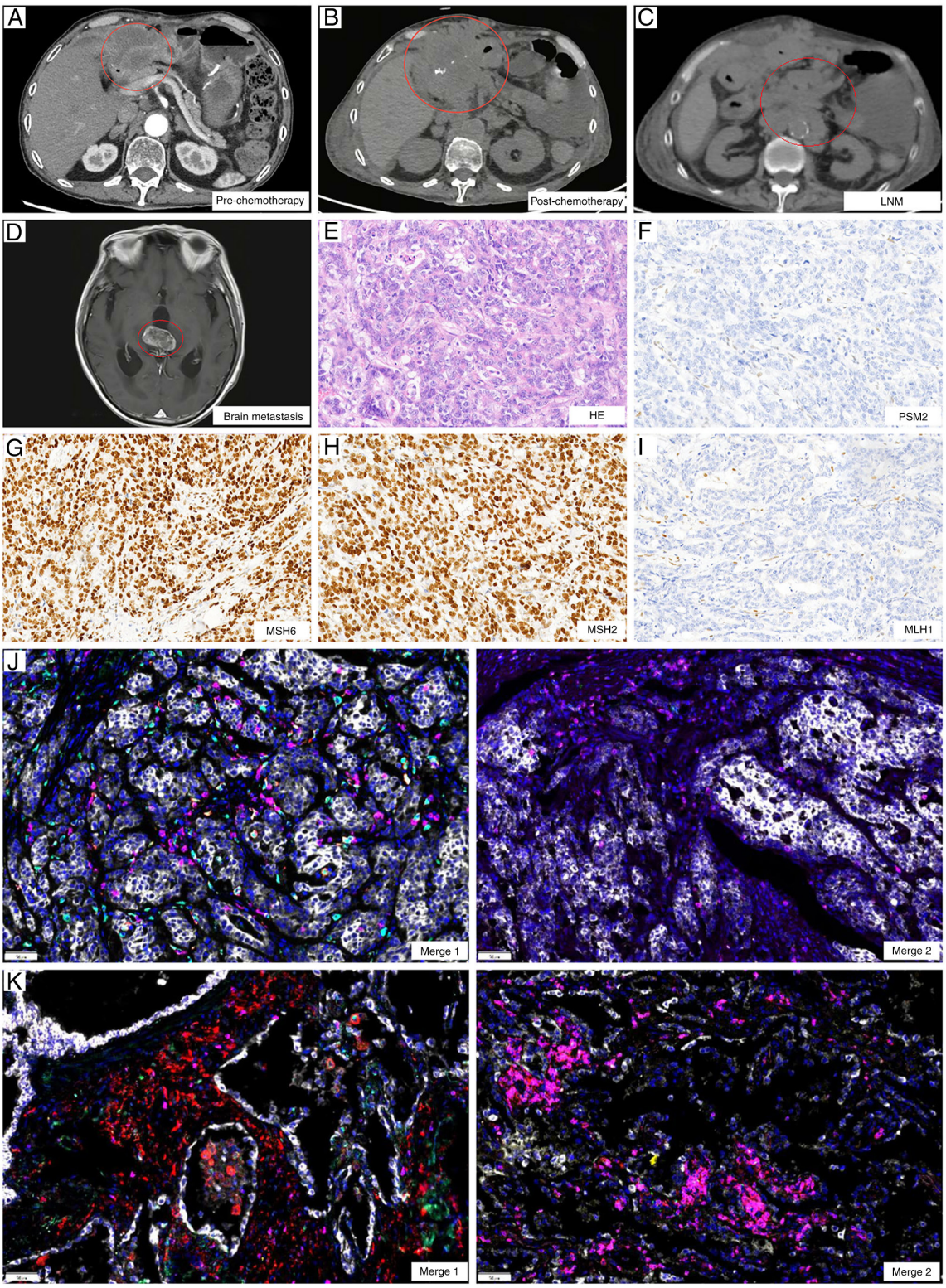

Figure 2. Imaging and immune microenvironment changes before and after treatment. CT images (A) before and (B) after treatment. (C) Lymph node metastases after treatment. (D) Brain metastases. Pathological examination of peritoneal puncture lesions, showing (E) HE staining and (F) PMS2, (G) MSH6, (H) MSH2 and (I) MLH1 protein detection, consistent with postoperative specimens (magnification, x100). Tumor immune microenvironment fusion images of (J) pre-treatment and (K) post-treatment (magnification, x200). Merge 1 shows PD-1 in green, programmed death-ligand 1 in yellow, CD8 in pink, CD68 in cyan and CD163 in red. Merge 2 shows CD3 in pink, CD4 in red, CD20 in green, CD56 in cyan and forkhead box P3 in yellow. PMS2, postmeiotic segregation increased (*S. Cerevisiae*) 2; MSH, MutS homolog; MLH1, MutL homolog.

Immune treatment cohorts. A total of three cohorts were analyzed: i) Kim cohort: Data was sourced from the Harvard Tumor Immune Dysfunction and Exclusion database (,including 61 patients with gastric cancer undergoing immunotherapy. After filtering for MSI status, 45 cases were retained: 5 MSI-H, 1 MSI-L and 39 MSS (14); ii) Peking University Cancer

Table II. Immune microenvironment assessment results summary: Tumor immune microenvironment cell composition.

A, Pre-treatment

	Count/mm², %	
Test index	Tumor parenchyma	Stroma
T cell-related		
CD3	19.40 (0.19)	83.40 (0.85)
$CD3^+CD4^+$	0.00 (0.00)	0.00 (0.00)
CD8	19.32 (0.19)	5.39 (0.08)
FoxP3	0.00 (0.00)	0.00 (0.00)
$PD\text{-}1^+CD8^+$	0.00 (0.00)	0.00 (0.00)
$CD3^+CD4^+FoxP3^+$	0.00 (0.00)	0.00 (0.00)
Macrophage-related		
$CD68^+CD163^+$	4.14 (0.04)	1.71 (0.02)
$CD68^+CD163^-$	57.78 (0.55)	57.59 (0.83)
$PD\text{-}L1^+$ $CD68^+$	2.24 (0.02)	3.11 (0.04)
NK cell-related		
CD56bright	0.00 (0.00)	0.00 (0.00)
CD56dim	0.00 (0.00)	0.00 (0.00)
B Cell-related		
CD20	0.02 (0.00)	2.38 (0.02)

B, Post-treatment

	Count/mm², %	
Test index	Tumor parenchyma	Stroma
T cell-related		
CD3	439.29 (5.45)	292.43 (3.59)
$CD3^+CD4^+$	95.06 (1.18)	54.84 (0.67)
CD8	6.68 (0.10)	3.00 (0.04)
FoxP3	0.00 (0.00)	0.18 (0.00)
$PD\text{-}1^+CD8^+$	0.00 (0.00)	0.00 (0.00)
$CD3^+CD4^+FoxP3^+$	0.00 (0.00)	0.00 (0.00)
Macrophage-related		
$CD68^+CD163^+$	0.00 (0.00)	0.00 (0.00)
$CD68^+CD163^-$	0.00 (0.00)	0.00 (0.00)
$PD\text{-}L1^+$ $CD68^+$	0.00 (0.00)	0.00 (0.00)
NK cell-related		
CD56bright	0.00 (0.00)	0.00 (0.00)
CD56dim	0.00 (0.00)	0.00 (0.00)
B cell-related		
CD20	17.07 (0.21)	0.86 (0.01)

FoxP3, forkhead box P3; PD-1, programmed death-1; PD-L1, programmed death-ligand 1; NK, natural killer.

Table III. Immune microenvironment assessment results summary: Tertiary lymphoid structure.

Group	Count/mm²	$\mu m^2/mm^2$
Pre-treatment	0.06	6,854.22
Post-treatment	0.00	0.00

'$\mu m^2/mm^2$' represents the area density unit, indicating the area size of tertiary lymphoid structures per unit area.

Hospital (PUCH) cohort: Data was obtained from the literature, comprising 39 patients with gastric cancer treated with immunotherapy (15); and iii) Esophagogastric Cancer-Memorial Sloan Kettering (EGC-MSK)-2017 cohort: Data was sourced from the aforementioned literature, including 30 patients with gastric cancer receiving immunotherapy (16). After filtering for MSI status, 28 cases were included: 5 MSI-H and 23 MSS.

Statistical analyses. Categorical variables (such as MSI subtype distribution in different stages and immunotherapy response between different MSI types) are summarized as frequencies (n), and the χ^2 test was used to assess intergroup comparisons. For continuous variables (such as TMB and neoantigen load), the Shapiro-Wilk test assessed normality. Subsequently, the normally distributed variables were evaluated using the unpaired t-test while non-normally distributed variables were analyzed using the Mann-Whitney U-test for two-group data. For multiple-group data, ANOVA was used followed by Tukey's post hoc test for normally distributed data, and the Kruskal-Wallis test was used followed by Dunn's multiple comparisons test as a non-parametric test. The abundance of TIME-related indicators was calculated using the CIBERSORT tool. Survival curves were generated using the Kaplan-Meier method, and intergroup survival differences were compared using the log-rank test. All statistical analyses were performed using R software (The R Foundation; version 4.4.1). $P<0.05$ was considered to indicate a statistically significant difference.

Results

Case report

Patient information and intervention. The patient, a 74-year-old man presented to the Southern University of Science and Technology Hospital (Shenzhen, China) in April 2022 with complaints of epigastric discomfort and anorexia for 2 months. CT revealed diffuse gastric wall lesions accompanied by multiple enlarged lymph nodes around the stomach, suggesting the possibility of infiltrative gastric cancer (data not shown). In April 2022, gastroscopy identified a large ulcer near the pylorus that bled easily upon palpation. Biopsy confirmed a diagnosis of poorly differentiated adenocarcinoma. In May 2022, following further examinations including contrast-enhanced thoracoabdominal computed tomography gastroscopy with biopsy, the patient underwent a radical gastrectomy. Post-surgical pathology analysis revealed a moderately-to-poorly differentiated gastric adenocarcinoma, categorized as diffuse type according to Lauren's classification (17). Cancer emboli were observed in blood vessels, and nerve involvement was also noted. Both surgical margins

Table IV. Age distribution by MS status in different cohorts.

A, EGC-MSK-2017 cohort

MSI status	n	Minimum	Quartile 1	Median	Mean	Quartile 3	Maximum
MSI-H	5	52.34	68.66	69.43	69.45	71.10	85.72
MSS	23	22.00	45.18	57.00	55.40	69.73	76.21

B, PUCH cohort

MSI status	n	Minimum	Quartile 1	Median	Mean	Quartile 3	Maximum
MSI-H	6	55.00	60.75	64.00	63.33	65.00	72.00
MSS	25	23.00	56.00	62.00	59.60	65.00	76.00

C, TCGA cohort

MSI status	n	Minimum	Quartile 1	Median	Mean	Quartile 3	Maximum
MSI-H	75	44.89	64.57	71.32	70.40	75.97	90.00
MSI-L	52	30.02	59.56	67.99	65.69	72.13	83.42
MSS	256	34.50	57.18	66.19	64.93	72.71	90.00

MSI, microsatellite instability; H, MSI-high; MSS, microsatellite stability; MSI-L, MSI-low; TCGA, The Cancer Genome Atlas; EGC-MSK-2017, Early Gastric Cancer-Memorial Sloan Kettering 2017 cohort; PUCH, Peking University Cancer Hospital cohort.

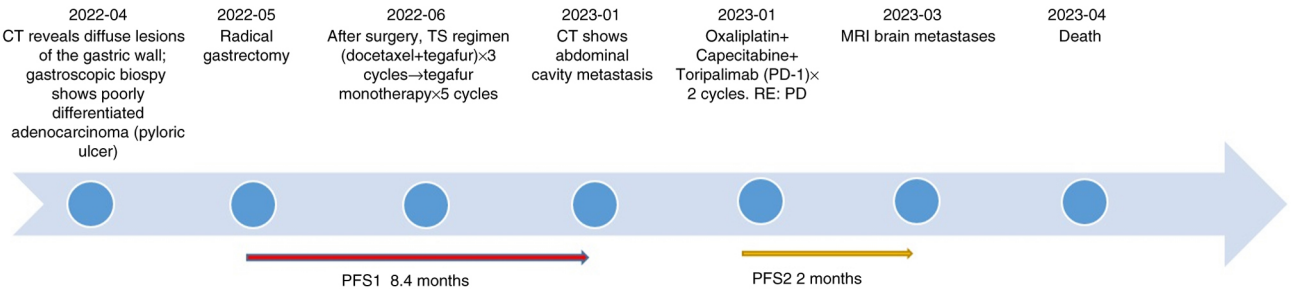

Figure 3. Clinical timeline of the disease course of the patient. Overall survival was 11.6 months. PFS, progression-free survival; PD, progressive disease; PD-1, programmed death-1, RE, response Evaluation.

were negative for cancer; however, lymph node metastasis was found in the surrounding adipose tissue (3/16). Metastases were observed in the 8th lymph node group (1/1), and the 1st and 3rd groups (3/5), while no metastases were observed in the 9th group (0/3). The immunohistochemistry results in accordance with standard clinical diagnostic protocols were as follows: MutL homolog 1 (-, deletion), postmeiotic segregation increased (*S. Cerevisiae*) 2 (-, deletion), MutS homolog (MSH)2 (+, no deletion), MSH6 (+, no deletion), CK7 (+), CK20 (-), C-erb-2 (0, negative) and EBER *in situ* hybridization (-), (Fig. 1; data for CK and Ki-67 are not shown)

The tumor was staged as pT4bN3aM0 according to the 8th edition of the American Joint Committee on Cancer staging system (18). Postoperatively, the patient received three cycles administered every three weeks (length of each cycle: 21 days) of chemotherapy of the TS regimen [docetaxel 75 mg/m^2 + tegafur 60 mg twice a day (bid)]. During treatment, the patient developed grade IV bone marrow suppression with infection, which improved after active management. Due to the advanced age of the patient and refusal of further aggressive chemotherapy, the patient was switched to single-agent tegafur (60 mg bid) for five cycles (length of each cycle: 21 days). administered every 3 weeks. The treatment was well-tolerated, and follow-up CT revealed no disease progression.

In January 2023, CT revealed abdominal metastases involving the peritoneum and lymph nodes (Fig. 2A and C), indicating disease progression. Therefore, 8 days later, the patient began treatment with oxaliplatin (130 mg/m^2) and capecitabine (1.5 g bid) in combination with the PD-1 inhibitor toripalimab. During the completion of two cycles administered every three weeks (length of each cycle: 21 days) of treatment, the patient experienced reduced appetite. Follow-up CT demonstrated continued lesion enlargement compared with January 2023 and disease progression was confirmed as per

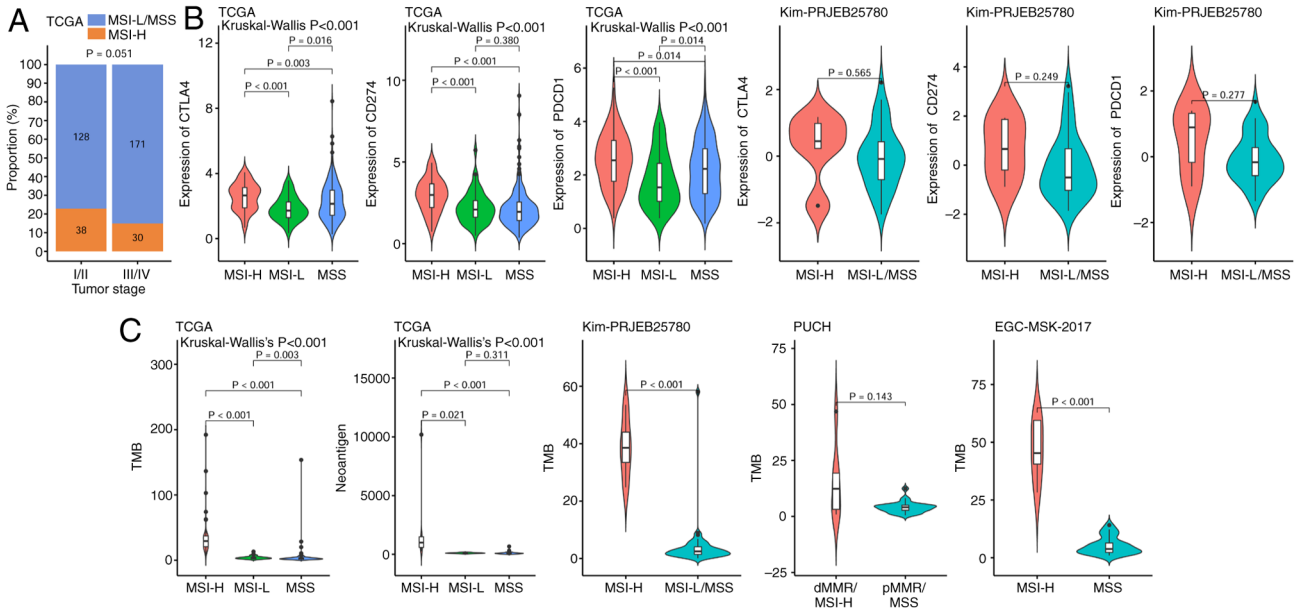

Figure 4. Association between MSI and gastric cancer staging. (A) Association between MSI and clinical stage in TCGA gastric cancer. (B) Association between MSI-H and immune checkpoint expression (CTLA4, CD274 and PDCD1) in different cohorts. (C) Association between MSI-H and TMB and neoantigen load in different cohorts. MSI, microsatellite instability; TCGA, The Cancer Genome Atlas; H, MSI-high; CTLA4, cytotoxic T-lymphocyte-associated protein 4; PDCD1, programmed cell death protein 1; TMB, tumor mutational burden; MSS, microsatellite stability; MSI-L, MSI-low.

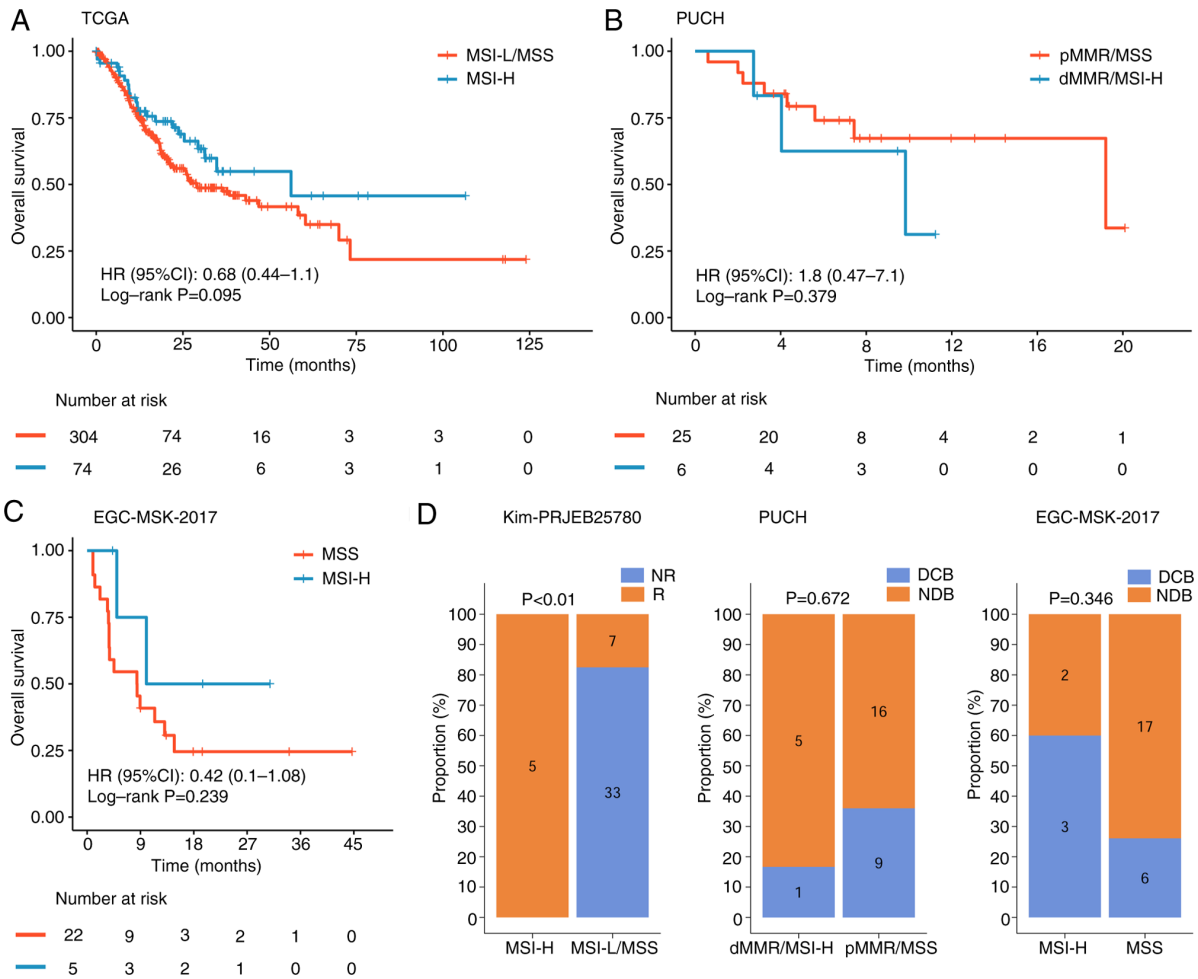

Figure 5. Prognostic differences between MSI-H and MSS groups across different databases. Survival analysis performed in the (A) TCGA, (B) PUCH and (C) EGC-MSK-2017 cohorts. (D) Immunotherapy response rates of patients with MSI-H in the Kim, PUCH and EGC-MSK-2017 cohorts. NR, not reported; R, response; MSI, microsatellite instability; H, MSI-high; MSS, microsatellite stability; TCGA, The Cancer Genome Atlas; HR, hazard ratio; CI, confidence interval; dMMR, deficient mismatch repair; MSI-L, MSI-low; pMMR proficient mismatch repair; DCB, Durable Clinical Benefit; NDB, Non-Durable Benefit.

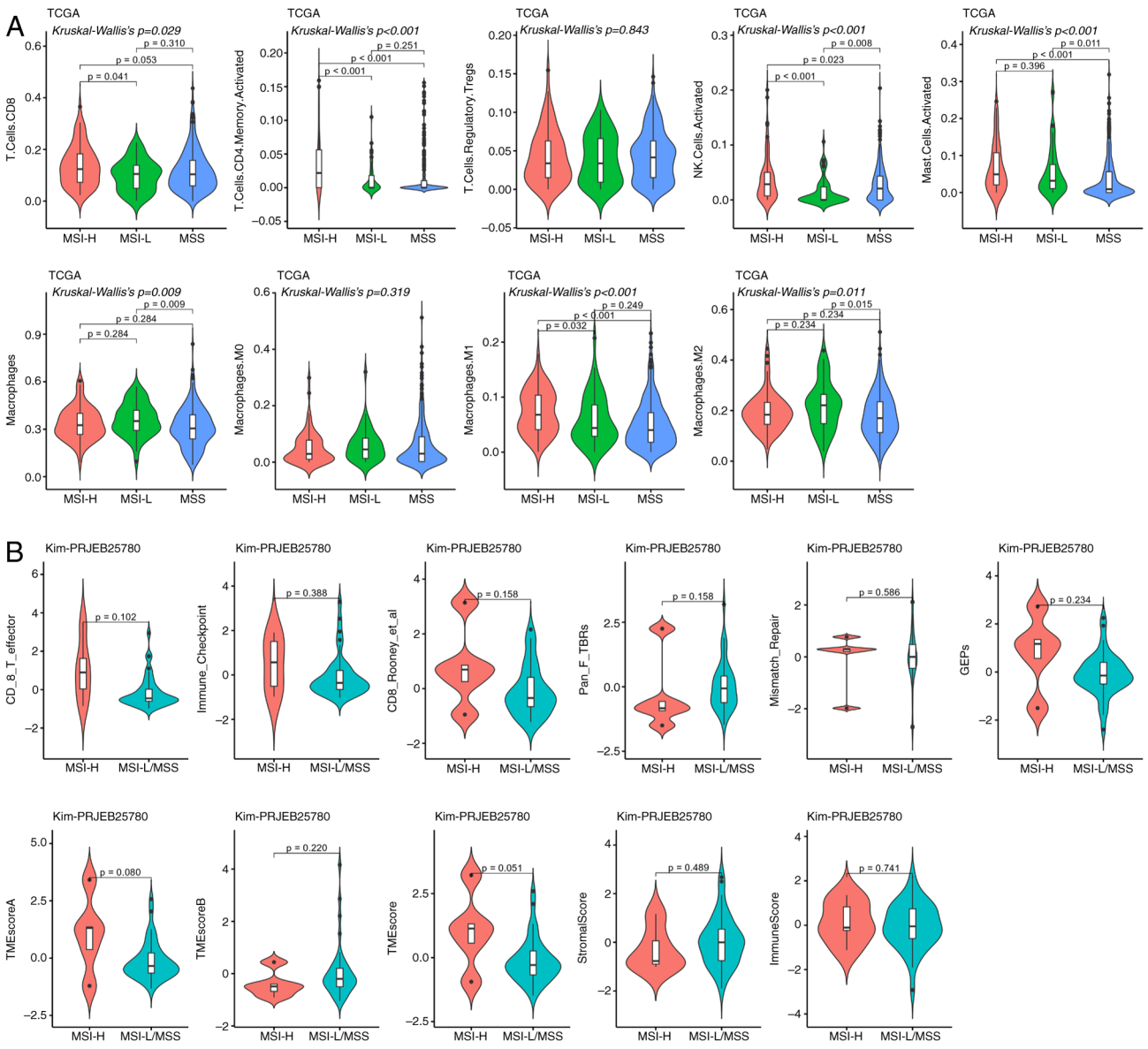

Figure 6. Differences in the immune microenvironment between MSI-H and MSS. (A) TCGA analysis demonstrated that patients with MSI-H exhibited significantly higher infiltration of memory-activated CD4$^+$ T cells, activated NK cells, mast cells and M1 macrophages than those with MSS; CD8$^+$ T cells showed a similar significant difference between the MSI-H and MSI-L groups (P<0.05). (B) Kim cohort analysis demonstrated no significant differences in detected immune-related indicators between MSI-H and MSS/MSI-L (P>0.05). MSI, microsatellite instability; MSI-H, MSI-high; MSS, microsatellite stability; TCGA, The Cancer Genome Atlas; NK, natural killer; MSI-L, MSI-low; NK, natural killer; TME, tumor microenvironment; M1, type 1 macrophages.

the Response Evaluation Criteria in Solid Tumors 1.1 criteria (Fig. 2A and B) (19). Although patients with dMMR gastric cancer typically respond favorably to immunotherapy (20) the treatment outcome of the patient in the present case was suboptimal, raising questions about whether tumor heterogeneity or other factors contributed to the poor response.

The abdominal metastases were located near the abdominal wall, and following patient consent, a biopsy of the lesions was performed to further characterize them. The biopsy results confirmed metastatic adenocarcinoma and dMMR status, consistent with baseline findings (Fig. 2E-I). To assess the potential underlying factors, both the postoperative pathological specimen and the post-treatment biopsy specimen underwent TIME-PRO assay.

TIME detection results. Before treatment, the TIME of the patient was deemed 'immune cold', characterized by low densities of CD3$^+$ T cells (19.4 cells/mm^2) and CD8$^+$ T cells (19.32 cells/mm^2), indicating a scarcity of total and effector T cells, well below the threshold for a strong immune response (CD8$^+$ T cell density, ≥330.1 cells/mm^2) (21). M1 macrophage density was also low (57.78 cells/mm^2) and forkhead box P3 (FoxP3)$^+$ regulatory T cells (Tregs), TLS and CD20$^+$ B cell counts were minimal, further confirming the low immune reactivity (Tables I-III; Fig. 2J).

After treatment, marked changes were observed. Although PD-L1 remained negative [tumor proportion score, <1%; combined positive score (CPS), <1], CD3$^+$ T cell density increased to 439.29 cells/mm^2, primarily due to CD3$^+$CD4$^+$ T cells (95.06 cells/mm^2), while CD8$^+$ T cells remained low (6.68 cells/mm^2), indicating a predominantly regulatory immune response. FoxP3$^+$ T cell density was 0.18 cells/mm^2, suggesting potential immune suppression. Meanwhile, B

cell infiltration did not notably increase ($CD20^+$ B cells, 17.07 cells/mm^2) and TLS remained absent. Overall, despite increased T cell infiltration, immune escape mechanisms and a suppressive microenvironment continued to limit effective antitumor immune responses, potentially compromising treatment efficacy (Tables I-III; Fig. 2K).

Follow-up. In March 2023, the patient developed changes in mental status, such as bradyphrenia and irrelevant answers to questions. Brain MRI revealed metastatic lesions (Fig. 2D), indicating poor disease control. The patient was provided with optimal nutritional support but died in April 2023 with an overall survival (OS) of 11.6 months (Fig. 3).

Bioinformatics results

Association between MSI and clinical Features. Table IV summarizes the age distribution of patients with gastric cancer stratified by MSI status across different cohorts. In the EGC-MSK-2017 cohort, patients in the MSI-H group were significantly older than those in the MSS group, while in the PUCH and TCGA cohorts, the age difference between the MSI-H and MSS groups was not significant Furthermore, the proportion of MSI-H patients with in gastric cancer stages I/II was notably higher compared with those with stages III/IV; however, statistical analysis revealed no significant difference between the groups (Fig. 4A).

Association between MSI and immune checkpoints. In TCGA gastric cancer cohort, the expression levels of the immune checkpoint markers cytotoxic T-lymphocyte-associated protein 4 (CTLA4), CD274 and programmed cell death protein 1 (PDCD1) were significantly higher in the MSI-H population compared with in the MSI-L and MSS populations. Similarly, in the Kim immunotherapy cohort, these markers were also notably elevated in the MSI-H group compared with in the MSS group, although the differences were not statistically significant, likely due to the small sample size of only five patients with MSI-H (Fig. 4B).

Association between MSI, TMB and neoantigen load. In TCGA gastric cancer cohort, the MSI-H group had a significantly higher TMB and neoantigen load than the MSI-L and MSS groups. Consistently, in the Kim and EGC-MSK-2017 immunotherapy cohorts, patients with MSI-H also showed a significantly higher TMB compared with those with MSI-L/MSS. Only the PUCH cohort demonstrated no significant difference in TMB between groups, possibly due to the small sample size (Fig. 4C).

Prognostic differences between MSI-H and MSS. In TCGA gastric cancer cohort, the MSI-H population showed a trend toward improved OS, with a hazard ratio (HR) of 0.68; however, the difference between the MSI-H and MSI-L/MSS populations was not statistically significant. In the PUCH immunotherapy cohort, OS did not differ significantly between MSI-H and MSS populations (HR, 1.8; log-rank P=0.379). Similarly, in the EGC-MSK-2017 cohort, patients with MSI-H exhibited a trend toward improved OS (HR, 0.42), but the difference was not statistically significant (log-rank P=0.239) (Fig. 5A-C).

Differences in immunotherapy response between MSI-H and MSS. Analysis of the Kim cohort demonstrated a significant difference in immunotherapy response between the MSI-H and MSS cohorts. By contrast, no significant difference was observed in the PUCH cohort between the dMMR/MSI-H and pMMR/MSS groups. In the EGC-MSK-2017 cohort, the MSI-H group exhibited a markedly higher durable clinical benefit rate, but this difference was not statistically significant compared with the MSS group (Fig. 5D).

Immune microenvironment differences between MSI-H and MSS. TCGA cohort revealed that, compared with the MSS population, patients with MSI-H had a significantly higher proportion of $CD4^+$ T cells, natural killer (NK) cells, mast cells and M1 macrophages. For $CD8^+$ T cells, a significant difference was only observed between MSI-H and MSI-L groups, with no difference detected between MSI-H and MSS groups (Fig. 6A). In the Kim cohort, no significant differences between MSI-H and MSS/LMSS groups were demonstrated for any of the detected immune-related indicators (Fig. 6B).

Discussion

The present study evaluated a patient with gastric cancer with dMMR features who did not respond to immunotherapy, by integrating multi-cohort bioinformatics data to elucidate the complex role of the immune microenvironment in treatment responses. Despite exhibiting a dMMR/MSI-H molecular profile, the tumor microenvironment displayed characteristics of a 'cold tumor', with very low PD-L1 expression (<1%), sparse tumor-infiltrating lymphocytes (TILs) and a modest accumulation of $FoxP3^+$ Treg cells. This suggests that although MSI-H status is typically considered a marker for sensitivity to immunotherapy, an immunosuppressive microenvironment can undermine its effectiveness.

In general, patients with dMMR gastric cancer tend to have a high TMB and a rich load of tumor neoantigens, which makes them more responsive to immune therapies (22). In TCGA and EGC-MSK-2017 cohorts, patients with MSI-H demonstrated a significantly higher TMB; however, this difference was not observed in the PUCH cohort, likely due to sample size limitations. In TCGA cohort, the MSI-H group generally displayed elevated expression of immune checkpoint markers (such as CTLA4, CD274 and PDCD1) as well as increased immune cell infiltration (such as $CD8^+$ T and NK cells), which could potentially serve as biomarkers for predicting immunotherapy outcomes.

Furthermore, despite the dMMR features of the tumor in the presented case, the immune microenvironment exhibited clear signs of immune inactivity, as demonstrated by low TIL levels and extremely low PD-L1 expression (<1%), indicating the presence of immune evasion mechanisms. Following treatment, although the number of $CD3^+$ T cells increased, there was no significant enhancement in $CD8^+$ T cell activity, and the accumulation of $FoxP3^+$ Treg cells in the tumor stroma further supported the notion that the immunosuppressive environment constrains effective immune responses (23). Furthermore, although there was an increase in $CD20^+$ B cells, their antitumor immune effects did not show notable enhancement. The marked accumulation of Treg cells and myeloid-derived suppressor cells (MDSCs), along with antigen presentation deficiencies, may have impaired the function of $CD8^+$ T cells, leading to an overall lack of immune activation (24). Moreover, the low expression of PD-L1 could contribute to the poor response to immunotherapy (25).

High TMB and dMMR status are typically considered strong predictors of immunotherapy response (20), yet the

present case, together with the cohort data, revealed considerable heterogeneity between these molecular features and clinical outcomes. Although the MSI-H cohort in TCGA study exhibited elevated immune checkpoint expression, the patient in the presented case had low PD-L1 expression, and variability observed in the Kim cohort suggests that the level of immune checkpoint expression may have an individual threshold effect. Only when this threshold (such as CPS ≥1) was surpassed did MSI-H features translate into therapeutic benefit. Therefore, personalized treatment strategies should account for immune microenvironment features and incorporate targeted therapies and chemotherapy to enhance immune responses.

The present case stands in contrast to the 'pro-inflammatory' phenotype (increased M1 macrophages) observed in the MSI-H group of TCGA cohort, suggesting functional heterogeneity within the MSI-H population regarding immune infiltration. While certain patients exhibit predominant immune infiltration by effector cells, others, such as the patient in the presented case, may experience immune suppression driven by regulatory cells, resulting in treatment resistance.

The Keynote-062 study reported that patients with dMMR have a markedly higher ORR (55%) compared with patients with pMMR (25%) (26). Moreover, in the Keynote-158 study, patients with dMMR reported an ORR of 50% (including a complete response of 15% and a partial response of 34%), while patients with pMMR had an ORR of 7%. In addition, the median PFS for patients with dMMR was 13.1 months, compared with 2.1 months for patients with pMMR (27). Nonetheless, 20-30% of patients with dMMR do not respond to immune therapy (28). The present case represents a 'non-responder', in which the immune microenvironment (low PD-L1 and high Treg/MDSCs) deviates from the general trends observed in the MSI-H cohort of TCGA study, yet aligns with reports of immune evasion mechanisms documented in other studies (29,30). This discrepancy may result from the interplay of several factors. On the one hand, dysregulated WNT/β-catenin pathway activation can impair neoantigen presentation, rendering high TMB tumors non-immunogenic. Notably, activated β-catenin stemming from dysregulated WNT pathways in dMMR tumors also suppresses TLS formation via downstream effects on the tumor microenvironment, specifically by modulating target molecules (such as c-Myc and cyclin D1) or interfering with the Wnt/TCF/lymphoid enhancer factor signaling axis (which regulates B cell chemokines such as chemokine (C-X-C motif) ligand 13, critical for TLS assembly) (31). This explains the sparse TILs observed in such cases. On the other hand, suppressive cells may directly inhibit $CD8^+$ T cell function through the secretion of factors such as TGF-β and IL-10 (32,33). Based on these findings, future predictive models should integrate genomic features such as MSI status and TMB, immune microenvironment composition such as $CD8^+$ T cell/Treg ratios, and dynamic functional indicators such as changes in PD-L1 expression, rather than relying on a single biomarker.

The present study highlights the importance of individualized TIME evaluation. While traditional biomarkers, such as dMMR and high TMB, predict the effectiveness of immune therapies, immunosuppressive mechanisms within the microenvironment may lead to treatment failure. Therefore, future strategies should explore combined approaches based on TIME characteristics and genomic profiles, such as novel antigen vaccines, adoptive T cell therapy, anti-VEGF drugs (such as bevacizumab) or Claudin 18.2-targeted monoclonal antibodies (such as zolbetuximab) that could reverse immune suppression and enhance efficacy (34,35). Claudin 18.2, a tight junction protein aberrantly expressed in 30-50% of gastric cancers, has emerged as a promising target for combination therapy with immunotherapy (33). This potential is further supported by data from two phase III clinical trials, SPOTLIGHT and GLOW, which reported that zolbetuximab in combination with chemotherapy markedly improved PFS and OS in patients with gastric cancer (36,37). However, as this agent was unavailable at the time of treatment, the patient in the presented case did not receive Claudin 18.2-targeted therapy, which may have contributed to the suboptimal response.

However, the present study has certain limitations, specifically the small number of cases included in the analysis may restrict the generalizability of the observed results regarding immune markers. Furthermore, the present study focused on descriptive associations between immune markers and clinical outcomes, without exploring the underlying biological mechanisms linking these markers to immunotherapeutic sensitivity in dMMR/MSI-H gastric cancer. Future studies should expand the study population to include a larger and more diverse cohort, and integrate functional experiments to elucidate the mechanistic basis, thereby identifying more optimal immune markers for clinical application.

In conclusion, the key conclusions of the present study are as follows: First, in dMMR/MSI-H gastric cancer (traditionally a subgroup with high TMB/neoantigen load favoring immunotherapy), TIME with low $CD8^+$ T cell infiltration, high $FoxP3^+$ Treg accumulation, absent TLS and low PD-L1 expression (<1%) is a critical indicator of immunotherapy resistance. This is exemplified by the presented non-responsive dMMR case. Second, cross-cohort analyses (TCGA-STAD, Kim, PUCH and EGC-MSK-2017) indicate that despite the generally favorable immunological features of MSI-H gastric cancers (such as higher TMB, $CD8^+$ T cells, M1 macrophages and immune checkpoints), their immunotherapy outcomes remain heterogeneous. Third, dMMR/MSI-H status alone is insufficient to predict immunotherapy responses; instead, individualized TIME evaluation (integrating $CD8^+$ T cell/Treg ratios, TLS presence and PD-L1 expression) is necessary for precise treatment guidance. Ultimately, combining genomic profiling (MSI and TMB) with TIME assessment may address treatment heterogeneity in dMMR/MSI-H gastric cancer and support exploring combined therapies (such as Claudin 18.2-targeted agents and anti-VEGF drugs) to reverse immunosuppression in non-responders.

Acknowledgements

Not applicable.

Funding

The present research was funded by the Major Science and Technology Project of Nanshan District Health and Wellness System (grant no. NSZD2024067).

Availability of data and materials

The data generated in the present study may be requested from the corresponding author.

Authors' contributions

LW contributed to the study conception and design, bioinformatics analyses, manuscript drafting, and integrated clinical bioinformatics data interpretation. XZ and MD contributed to clinical data acquisition and verification, clinical-molecular feature association analysis, and drafting of the clinical section of the manuscript. WD contributed to pathological data provision and pathology-molecular subtype association interpretation. LW and WD confirm the authenticity of all the raw data. All authors read and approved the final manuscript.

Ethics approval and consent to participate

The present study was reviewed and approved by the Ethical Review Committee of Southern University of Science and Technology Hospital [approval no. 2023(12)]. The patient provided written informed consent for the use of their samples and data in the present study.

Patient consent for publication

The patient provided written informed consent for the publication of this manuscript, including the use of any potentially identifiable data and images.

Competing interests

The authors declare that they have no competing interests.

References

1. Sung H, Ferlay J, Siegel R, Laversanne M, Soerjomataram I, Jemal A and Bray F: Global cancer statistics 2020: GLOBOCAN Estimates of incidence and mortality worldwide for 36 cancers in 185 countries. CA Cancer J Clin 71: 209-249, 2021.
2. Zhang TC, Chen H, Yin X, He Q, Man J, Yang X and Lu M: Changing trends of disease burden of gastric cancer in China from 1990 to 2019 and its predictions: Findings from Global Burden of Disease Study. Chin J Cancer Res 33: 11-26, 2021.
3. Wang J, Xiu J, Farrell A, Battaglin F, Arai H, Millstein J, Soni S, Zhang W, Shields A, Grothey A, *et al*: Genomic landscapes to characterize mismatch-repair deficiency (dMMR)/microsatellite instability-high (MSI-H) gastrointestinal (GI) cancers stratified by tumor mutation burden (TMB). J Clin Oncol 41 (16 Suppl): S2618-S2618, 2023.
4. Le DT, Durham JN, Smith KN, Wang H, Bartlett BR, Aulakh LK, Lu S, Kemberling H, Wilt C, Luber BS, *et al*: Mismatch repair deficiency predicts response of solid tumors to PD-1 blockade. Science 357: 409-413, 2017.
5. Petrelli F, Antista M, Marra F, Cribiù F, Rampulla V, Pietrantonio F, Dottorini L, Ghidini M, Luciani A, Zaniboni A and Tomasello G: Adjuvant and neoadjuvant chemotherapy for MSI early gastric cancer: A systematic review and meta-analysis. Ther Adv Med Oncol 16: 1948-1957, 2024.
6. Takei S, Kawazoe A and Shitara K: The new era of immunotherapy in gastric cancer. Cancers (Basel) 14: 1054, 2022.
7. Zhang P and Gou H: Immunotherapy-based therapy versus chemotherapy for the neoadjuvant treatment of locally advanced dMMR/MSI-H gastric cancer. J Clin Oncol 42 (16_suppl): e16121, 2024.
8. Mou P, Ge Q, Sheng R, Zhu T, Liu Y and Ding K: Research progress on the immune microenvironment and immunotherapy in gastric cancer. Front Immunol 14: 1291117, 2023.
9. Marcus L, Lemery S, Keegan P and Pazdur R: FDA approval summary: Pembrolizumab for the treatment of microsatellite Instability-High solid tumors. Clin Cancer Res 25: 3753-3758, 2019.
10. Hu L, Li T, Deng S, Gao H, Jiang Y, Chen Q, Chen H, Xiao Z, Shuai X and Su Z: Tertiary lymphoid structure formation induced by LIGHT-engineered and photosensitive nanoparticles-decorated bacteria enhances immune response against colorectal cancer. Biomaterials 314: 122846, 2025.
11. Fridman W, Sibéril S, Pupier G, Soussan S and Sautès-Fridman C: Activation of B cells in Tertiary Lymphoid Structures in cancer: Anti-tumor or anti-self? Semin Immunol 65: 101703, 2023.
12. Wang FH, Zhang XT, Li YF, Tang L, Qu XJ, Ying JE, Zhang J, Sun LY, Lin RB, Qiu H, *et al*: Clinical guidelines for the diagnosis and treatment of gastric cancer. Cancer Commun 41: 747-795, 2021.
13. Cancer Genome Atlas Research Network: Comprehensive molecular characterization of gastric adenocarcinoma. Nature 513: 202-209, 2014.
14. Kim ST, Cristescu R, Bass AJ, Kim KM, Odegaard JI, Kim K, Liu XQ, Sher X, Jun H, et al. Comprehensive molecular characterization of clinical responses to PD-1 inhibition in metastatic gastric cancer. Nat Med 24: 1449-1458, 2018.
15. Jiao X, Wei X, Li S, Liu C, Chen H, Gong J, Li J, Zhang X, Wang X et al. A genomic mutation signature predicts the clinical outcomes of immunotherapy and characterizes immunophenotypes in gastrointestinal cancer. NPJ Precis Oncol. 5: 36, 2021.
16. Janjigian YY, Sanchez-Vega F, Jonsson P, Chatila WK, Hechtman JF, Ku GY, Riches JC, Tuvy Y, Kundra R, Bouvier N, *et al*: Genetic predictors of response to systemic therapy in esophagogastric cancer. Cancer Discov 8: 49-58, 2018.
17. Lauren P: The two histological main types of gastric carcinoma: Diffuse and so-called intestinal-type carcinoma. An attempt at a Histo-clinical classification. Acta Pathol Microbiol Scand 64: 31-49, 1965.
18. American Joint Committee on Cancer (AJCC). AJCC Cancer Staging Manual, 8th edition. Edge SB, Byrd DR, Compton CC, *et al* (eds.): New York, Springer, 2017.
19. Eisenhauer EA, Therasse P, Bogaerts J, Schwartz LH, Sargent D, Ford R, Dancey J, Arbuck S, Gwyther S, Mooney M, *et al*: New response evaluation criteria in solid tumours: Revised RECIST guideline (version 1.1). Eur J Cancer 45: 228-247, 2009.
20. André T, Tougeron D, Piessen G, de la Fouchardière C, Louvet C, Adenis A, Jary M, Tournigand C, Aparicio T, Desrame J, *et al*: Neoadjuvant nivolumab plus ipilimumab and adjuvant nivolumab in localized deficient mismatch Repair/Microsatellite Instability-high gastric or esophagogastric junction adenocarcinoma: The GERCOR NEONIPIGA Phase II study. J Clin Oncol 41: 255-265, 2023.
21. Obeid J, Hu Y, Erdag G, Leick K and Slingluff C: The heterogeneity of tumor-infiltrating CD8+ T cells in metastatic melanoma distorts their quantification: How to manage heterogeneity? Melanoma Res 27: 211-217, 2017.
22. Ma W, Pham B and Li T: Cancer neoantigens as potential targets for immunotherapy. Clin Exp Metastasis 39: 51-60, 2022.
23. Hugo W, Zaretsky J, Sun L, Song C, Moreno B, Hu-Lieskovan S, Berent-Maoz B, Pang J, Chmielowski B, Cherry G, *et al*: Genomic and transcriptomic features of response to Anti-PD-1 therapy in metastatic melanoma. Cell 165: 35-44, 2016.
24. Garon EB, Rizvi NA, Hui R, Leighl N, Balmanoukian AS, Eder JP, Patnaik A, Aggarwal C, Gubens M, Horn L, *et al*: Pembrolizumab for the treatment of non-small-cell lung cancer. N Engl J Med 372: 2018-2028, 2015.
25. De Fátima Aquino Moreira-Nunes C, De Souza Almeida Tita n Martins C, Feio D, Lima IK, Lamarão LM, de Souza CRT, Costa IB, da Silva Maués JH, Soares PC, de Assumpção PP and Burbano RMR: PD-L1 expression associated with Epstein-Barr virus status and Patients' survival in a large cohort of gastric cancer patients in northern brazil. Cancers (Basel) 13: 3107, 2021.
26. Shitara K, Van Cutsem E, Bang YJ, Fuchs C, Wyrwicz L, Lee KW, Kudaba I, Garrido M, Chung HC, Lee J, *et al*: Efficacy and safety of pembrolizumab or pembrolizumab plus chemotherapy vs chemotherapy alone for patients With First-line, advanced gastric cancer: The KEYNOTE-062 phase 3 randomized clinical trial. JAMA Oncol 6: 1571-1580, 2020.
27. O'Malley DM, Bariani GM, Cassier PA, Marabelle A, Hansen AR, Acosta AJ, Miller WH Jr, Safra T, Italiano A, Mileshkin L, *et al*: Pembrolizumab in microsatellite instability-high/mismatch repair deficient (MSI-H/dMMR) and non-MSI-H/non-dMMR advanced endometrial cancer: Phase 2 KEYNOTE-158 study results. Gynecol Oncol 193: 130-135, 2025.
28. Overman MJ, McDermott R, Leach JL, Lonardi S, Lenz HJ, Morse MA, Desai J, Hill A, Axelson M, Moss RA, *et al*: Nivolumab in patients with metastatic DNA mismatch repair-deficient or microsatellite instability-high colorectal cancer (CheckMate 142): An open-label, multicentre, phase 2 study. Lancet Oncol 18: 1182-1191, 2017.

29. Zeng D, Wu J, Luo H, Li Y, Xiao J, Peng J, Ye Z, Zhou R, Yu Y, Wang G, *et al*: Tumor microenvironment evaluation promotes precise checkpoint immunotherapy of advanced gastric cancer. J Immunother Cancer 9: e002467, 2021.
30. Li N, Li Y, Li J, Tang S, Gao H and Li Y: Correlation of the abundance of MDSCs, Tregs, PD-1, and PD-L1 with the efficacy of chemotherapy and prognosis in gastric cancer. Lab Med 56: 259-270, 2025.
31. Kim Y, Bae YJ, Kim JH, Kim H, Shin SJ, Jung DH and Park H: Wnt/β-catenin pathway is a key signaling pathway to trastuzumab resistance in gastric cancer cells. BMC Cancer 23: 922, 2023.
32. Bernal M, Ruiz-Cabello F, Concha A, Paschen A and Garrido F: Implication of the β2-microglobulin gene in the generation of tumor escape phenotypes. Cancer Immunol Immunother 61: 1359-1371, 2012.
33. Moaaz M, Lotfy H, Elsherbini B, Motawea M and Fadali G: TGF-β enhances the Anti-inflammatory effect of Tumor-infiltrating CD33+11b+HLA-DR Myeloid-derived suppressor cells in gastric cancer: A possible relation to MicroRNA-494. Asian Pac J Cancer Prev 21: 3393-3403, 2020.
34. Niu Q, Liu J, Luo X, Su B and Yuan X: Future of targeted therapy for gastrointestinal cancer: Claudin 18.2. Oncol Transl Med 17: P102-P107, 2021.
35. Zhang D, Huang G, Liu J and Wei W: Claudin18.2-targeted cancer theranostics. Am J Nucl Med Mol Imaging 13: 64-69, 2023.
36. Shitara K, Lordick F, Bang YJ, Enzinger P, Ilson D, Shah MA, Van Cutsem E, Xu RH, Aprile G, Xu J, *et al*: Zolbetuximab plus mFOLFOX6 in patients with CLDN18.2-positive, HER2-negative, untreated, locally advanced unresectable or metastatic gastric or gastro-oesophageal junction adenocarcinoma (SPOTLIGHT): A multicentre, randomised, double-blind, phase 3 trial. Lancet 401: 1655-1668, 2023.
37. Shah MA, Shitara K, Ajani JA, Bang YJ, Enzinger P, Ilson D, Lordick F, Van Cutsem E, Gallego Plazas J, Huang J, *et al*: Zolbetuximab plus CAPOX in CLDN18.2-positive gastric or gastroesophageal junction adenocarcinoma: The randomized, phase 3 GLOW trial. Nat Med 29: 2133-2141, 2023.